PNAS RESEARCH ARTICLE | CHEMISTRY

Size-dependent charge transfer between water microdroplets

Shiquan Lin[a,b,1], Leo N. Y. Cao[a,b,1], Zhen Tang[a,b], and Zhong Lin Wang[a,b,c,d,2]

Edited by Richard Zare, Stanford University, Stanford, CA; received May 17, 2023; accepted June 26, 2023

Contact electrification (CE) in water has attracted much attention, owing to its potential impacts on the chemical reactions, such as the recent discovery of spontaneous generation of hydrogen peroxide (H_2O_2) in water microdroplets. However, current studies focus on the CE of bulk water, the measurement of CE between micrometer-size water droplets is a challenge and its mechanism still remains ambiguous. Here, a method for quantifying the amount of charge carried by the water microdroplets produced by ultrasonic atomization is proposed. In the method, the motions of water microdroplets in a uniform electric field are observed and the electrostatic forces on the microdroplets are calculated based on the moving speed of the microdroplets. It is revealed that the charge transfer between water microdroplets is size-dependent. The large microdroplets tend to be positively charged while the small microdroplets tend to receive negative charges, implying that the negative charges transfer from large microdroplets to the small microdroplets during ultrasonic atomization. Further, a theoretical model for microdroplets charging is proposed, in which the curvature-induced surface potential/energy difference is suggested to be responsible for the charge transfer between microdroplets. The findings show that the electric field strength between two microdroplets with opposite charges during separation is strong enough to convert OH^- to OH^*, providing evidence for the CE-induced spontaneous generation of H_2O_2 in water microdroplets.

contact electrification | water droplets | size-dependent | liquid–liquid interface

Contact electrification (CE) is one of the most mysterious physical phenomena that occurs at almost any material contact interface, which is responsible for the charging of small solid particles in such as sand storms and fluidized beds (1, 2). The charging of liquid microdroplets is also common in nature, such as in the electrification of thunderstorms and fogs (3). The charge transfer between chemically identical solid particles has been widely discussed (4, 5). It was revealed that the charge transfer of the solid particles is size-dependent, the small solid particles tend to receive negative charges and large solid particles tend to be positively charged in the CE of multiparticle systems (6). However, the charge transfer between chemically identical liquid microdroplets was rarely mentioned owing to the lack of relevant control and detection techniques, leading to a poor understanding of the formation of the charged liquid microdroplets in nature.

Revealing the mechanism of CE between liquid microdroplets also has implications for understanding microdroplet chemistry (7–11). Over the past decade, the chemical properties of the liquid micro/nanodroplets were demonstrated to be very different from that of the bulk liquid (12, 13), and a large number of studies have shown that many chemical reactions in micrometer-sized water droplets are several orders of magnitude faster compared to that in the bulk phase water (14–18). The rapid chemical reactions in microdroplets have important applications in chemical synthesis (19–22), materials science (23, 24), and biological science (25–27), but the mechanism of microdroplet chemistry is not fully understood (14, 28). The surface electric fields were recently confirmed to be one of the sources of the accelerated reaction in microdroplets (29–32), implying that the surface electric field induced by the CE between microdroplets may contribute to the microdroplet chemical reaction (33). A typical microdroplet chemical reaction is introduced here to better illustrate the importance of CE to the chemical reaction. Very recently, it was reported that water will be oxidized by atomizing bulk water into micrometer-sized droplets and spontaneously producing hydrogen peroxide (H_2O_2) without external electric field (34–39). This is an exciting discovery which provides innovative opportunities for self-cleaning of surface and safe disinfection. It also gives a new clue for the generation of the O_2 molecules in the prebiotic period (38, 39). However, the mechanism of the spontaneous generation of H_2O_2 is still under debate and a potential explanation was proposed that the strong electric field at the periphery of water microdroplet assists the conversion of OH^- to OH^* and further generates H_2O_2 (38, 39). In addition, the CE-induced charging of the water microdroplets may be responsible for the generation of the strong electric field at the periphery, which indicates that the CE could be the fundamental driving force for the spontaneous generation

Significance

A method for quantifying the charges carried by water microdroplets in fog is designed. The size-dependent charge transfer between water microdroplets is discovered. It is revealed that the electric field strength between two microdroplets with opposite charges during separation reaches ~10^9 V/m, which is strong enough to drive the chemical reactions, such as the spontaneous generation of H_2O_2 in the water microdroplets. The results suggest that the contact electrification could be one of the driving forces for the accelerated chemical reaction in microdroplets, and the size-dependent charge transfer between water microdroplets provides a new perspective to understand the size-dependent chemical reaction rates in microdroplet chemistry. The findings have important implications for sonochemistry, microdroplet chemistry, chemical synthesis, and electrochemistry.

Author contributions: S.L. and Z.L.W. designed research; S.L. performed research; S.L., L.N.Y.C., Z.T., and Z.L.W. analyzed data; and S.L., L.N.Y.C., Z.T., and Z.L.W. wrote the paper.

The authors declare no competing interest.

This article is a PNAS Direct Submission.

[1]S.L. and L.N.Y.C. contributed equally to this work.

[2]To whom correspondence may be addressed. Email: zlwang@gatech.edu.

This article contains supporting information online at https://www.pnas.org/lookup/suppl/doi:10.1073/pnas.2307977120/-/DCSupplemental.

Published July 24, 2023.

of H_2O_2 in the water microdroplets (36). Therefore, it is of great significance to investigate the charge transfer mechanism between water microdroplets for the CE-induced chemical reactions, such as the spontaneous generation of H_2O_2.

In this paper, the water microdroplets were generated by ultrasonic nebulization, and the amount of charge carried by the microdroplets was measured by observing the movement of the microdroplets in a uniform electric field. The size distribution and carried charges of the water microdroplets were measured by using Kelvin probe force microscopy (KPFM). It is shown that the small microdroplets tend to receive negative charges while the large microdroplets tend to be positively charged in the ultrasonic nebulization, which is consistent with the reported cases with chemically identical solid particles. Based on the curvature-induced energy shift of the microdroplets, a theoretical model to explain the size-dependent charge transfer between water microdroplets is proposed here. The findings provide experimental evidence for the charging of the microdroplets, supporting the CE-induced spontaneous generation of H_2O_2 and having implications for sonochemistry and microdroplet chemistry.

Results

The Measurement Principle of Charges Carried by the Water Microdroplets. The measurement of the droplet charges has always been an important topic. In addition to using a Faraday cup (40, 41), an effective way to measure droplet charge is to place the droplet in a uniform electric field (42–45) and then obtain the droplet charge by observing the electric field force received by the droplet, such as the famous Millikan experiment (43, 44) and recent studies about CE between water and hydrophobic surfaces (45). Similar to these experiments, we designed a method to measure the amount of charge carried by the fog microdroplets. In our method, an ultrasonic atomizer was placed below the gap of two parallel electrodes (50 cm apart), as shown in Fig. 1*A*. The deionized water (DI water) was atomized and the fog microdroplets will move upward and into the gap between two electrodes. When constant voltages were applied on the electrodes, a stable electric field will be established between the two electrodes and the charged microdroplets will experience electrostatic force. As shown in Fig. 1*B*, the electrostatic forces on the negatively and positively charged microdroplets are toward the positive and negative electrodes, respectively. Therefore, the polarity of the charge carried by the microdroplets can be obtained by observing the moving direction of the microdroplets in the electric field. When the fog microdroplets begin to move due to the electrostatic force, the microdroplets will experience a drag force, which is opposite to the electrostatic force (46). It was demonstrated that the charged particle and microdroplet in the electric field will accelerate and, due to the balance of electric force and drag force, quickly reach

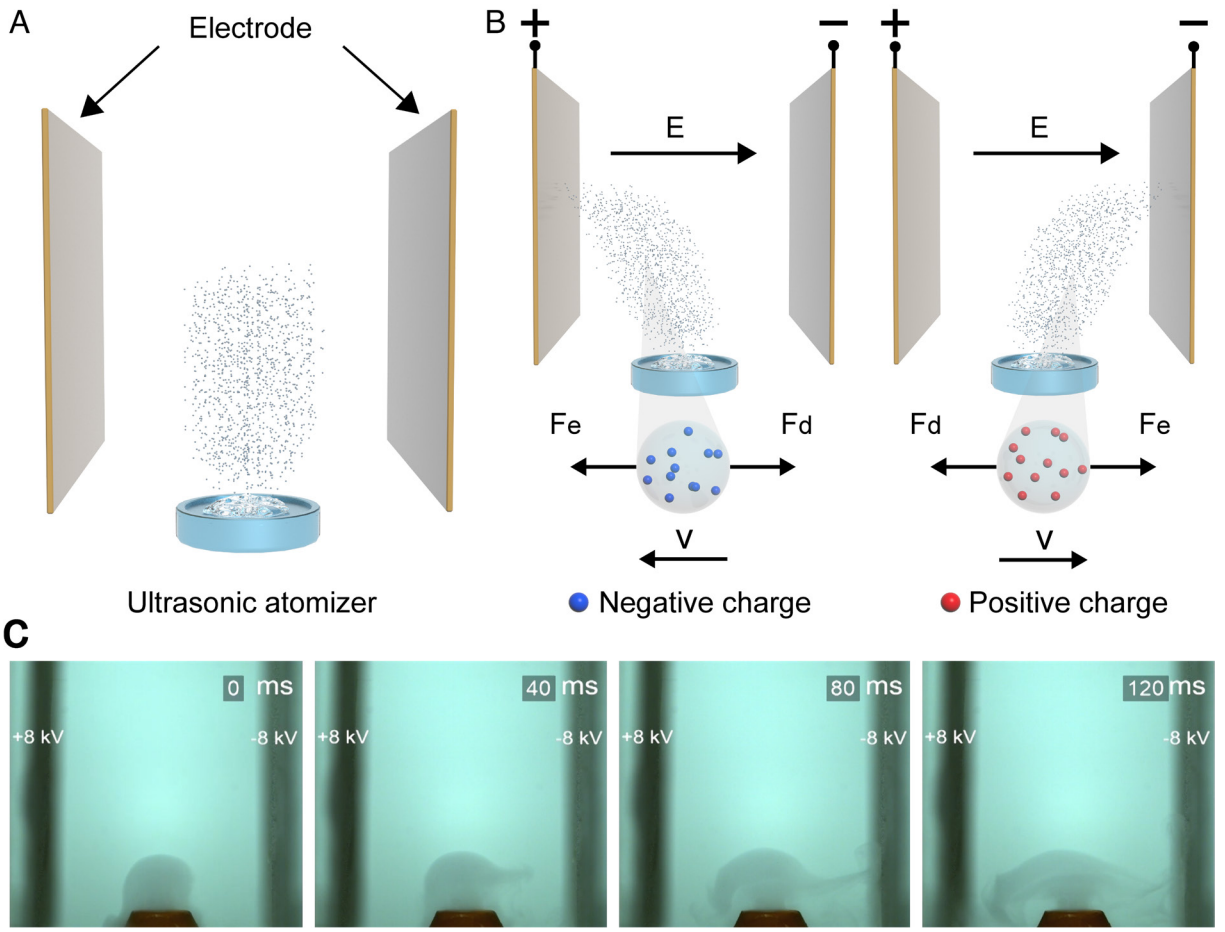

Fig. 1. The setup of the experiments. (*A*) The schematic diagram of the experiment set. An ultrasonic atomizer is placed below the gap of two parallel electrodes, which are 50 cm apart. (*B*) The schematic for the movement and force analysis of the negatively charged and positively charged water microdroplet in the uniformed electric field. The negatively charged microdroplet will move toward the positive electrode while the positively charged will move toward the negative electrode owing to the opposite's attraction. F_e denotes the electrostatic force on the microdroplet, and F_d denotes the drag force on the microdroplet. (*C*) The movement of the fog microdroplets taking by the high-speed camera, when the two electrode potentials are 8 kV and −8 kV, respectively.

a stable velocity, which is called the terminal electrostatic velocity (V_{TE}) and can be calculated by (47)

$$V_{TE} = \frac{neEC_c}{3\pi\eta d}, \quad [1]$$

where n is number of elementary charges, e is elementary charge, E is electric field strength, C_c is Cunningham correction factor, η is air viscosity, and d is microdroplet diameter.

Here, the Cunningham correction factor (C_c) has many forms depending on the regions (48). Since the Reynolds number (Re) described in the following equation in our case is estimated to be much less than 1, the situation lies in the Stokes' region (47).

$$Re = \frac{\rho_{air} V_{TE} d}{\eta}, \quad [2]$$

where ρ_{air} is the air density.

For Stokes' region, the Cunningham correction factor is calculated by (47)

$$C_c = 1 + \frac{2.52\lambda}{d}, \quad [3]$$

where λ is mean free path of air molecule.

Combining Eqs. **1** and **3**, the amount of charge (q) carried by the microdroplet can be calculated by

$$q = ne = \frac{V_{TE} 3\pi\eta d^2}{E(d + 2.52\lambda)}. \quad [4]$$

In Eq. **4**, the air viscosity (η), electric field strength (E), and mean free path of air molecule (λ) are known. If the two unknowns (V_{TE} and d) are measured, the amount of charge carried by microdroplets can be obtained. Here, the terminal electrostatic velocity (V_{TE}) is measured and calculated by using a high-speed camera. As shown in Fig. 1*C* and Movie S1, the fog microdroplets were separated into two parts and attracted by the electrodes when the 8 kV and −8 kV potentials were applied. This implies that there are both positive and negative microdroplets in ultrasonic atomization. By observing the video and measuring the moving distance of the fog microdroplets within a certain time, the terminal electrostatic velocity of microdroplets can be obtained by dividing the traveling distance by time.

Measuring the Water Microdroplets Size Distribution. Measuring size distribution of the collected volatile microdroplets is a challenging task. At present, the size distribution of the collected microdroplets is usually measured by cascade impactors. However, the method measures the aerodynamic diameter instead of geometric diameter and the droplet evaporation heavily affects further analysis. In this work, we proposed a new method for measuring the microdroplet size, which is based on the KPFM method. As shown in Movie S2, a polytetrafluoroethylene (PTFE) film coated on the conductive Si surface was used to collect the water microdroplets. As the PTFE film approaches the fog, the water microdroplets adhere to the PTFE surface and then evaporate away. During the evaporation, the charge transfer occurs between the water microdroplets and PTFE film, and the circular charge pattern is left on the PTFE surface. As shown in Fig. 2*A*, the diameter of the circular charge pattern (d'), which is also the diameter of the contact region between water microdroplet and PTFE film, can be directly measured by using KPFM (the principle of the KPFM for surface charge measurement has been introduced elsewhere) (49). According to the geometric and the volume conservation of the microdroplets before and after the adsorption, the diameter of the microdroplets (d) before adsorption on the PTFE surface is calculated to be (the calculation details are shown in *SI Appendix*, Fig. S1 and *Supplementary note 1*)

$$d = d'^3\sqrt{1 - \frac{1}{2}\left(\frac{1}{\sin(\pi-\theta)}\right)^2\left(\frac{1}{\sin(\pi-\theta)} - \frac{1}{\tan(\pi-\theta)}\right) + \frac{1}{4\tan(\pi-\theta)}} \quad [5]$$

where θ denotes the water contact angle of the PTFE film, which was measured to be 104° (*SI Appendix*, Fig. S2). Then, we have $d = 0.87d'$.

Fig. 2*B* gives four charge patterns on the PTFE surface after contact with microdroplets with different diameters. The diameters of the circular charge pattern are directly measured to be 1 μm, 3 μm, 4 μm, and 6 μm, corresponding to microdroplet diameters in 0.87 μm, 2.61 μm, 3.48 μm, and 5.22 μm, respectively. It is noted that the periphery of the patterns is negative and the middle region is positive, which is related to the evaporation of water microdroplets on the PTFE surface. As shown in *SI Appendix*, Fig. S3, the water microdroplets shrink under the action of surface tension at the initial stage of evaporation, and there is mutual sliding between the microdroplets boundary and PTFE. In this stage, negative charges are transferred from the microdroplets to the PTFE surface and microdroplets are positively charged, so the periphery of the charge pattern is negative. In the next stage, the microdroplets evaporate directly without shrinking, leaving the positive charges on the PTFE surface, so that the middle region of the charge pattern is positive. Although evaporation may carry away the charge, we can still estimate the charge of the microdroplets by calculating the average Kelvin potential ($\overline{V}$) of the charge pattern, which is −56 mV, 10 mV, 43 mV, and 72 mV for microdroplets with 0.87 μm, 2.61 μm, 3.48 μm, and 5.22 μm diameter, respectively (Fig. 2*B*). The results give the first clue that large microdroplets more likely to be positively charged compared to small microdroplets in ultrasonic atomization.

To measure the accurate amount of charge carried by the microdroplet and verify the size-dependent charging of microdroplets in ultrasonic atomization, the diameter distribution of the microdroplets was calculated. Fig. 2*C* gives the charge patterns of the fog microdroplets generated by the ultrasonic atomizer with 1.7 MHz frequency. We counted the diameter over 200 microdroplets and its corresponding distribution is shown in Fig. 2*F*. It is shown that the average diameter of the microdroplets generated by a 1.7-MHz ultrasonic atomizer is about 2.6 μm. This result is consistent with the ultrasonic atomization theory, in which the average diameter of the water microdroplets can be calculated by (50)

$$d_a = 0.34\left(\frac{8\pi\sigma}{\rho_{water} f^2}\right)^{1/3}, \quad [6]$$

where d_a denotes the average diameter of microdroplets, σ is the surface tension of the DI water, ρ_{water} is the density of DI water, and f is the frequency of the ultrasonic atomizer. By applying all the parameters of water in Eq. **6**, the average diameter of the water microdroplets was calculated to be exactly 2.6 μm, which verified the validity of our KPFM method for measuring the diameter of water microdroplets.

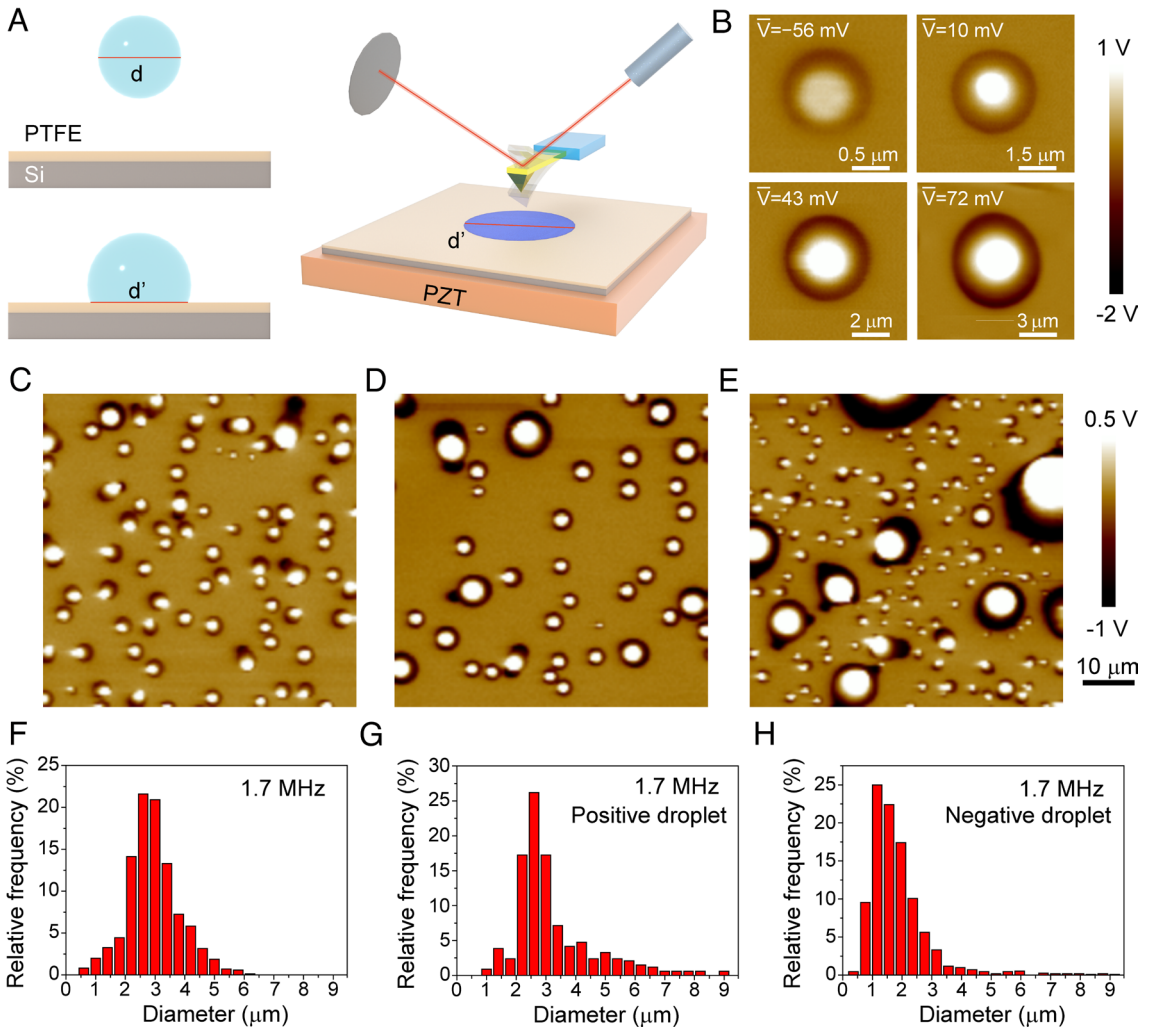

Fig. 2. Measurement of the water microdroplet diameters. (*A*) The measurement of the diameter of circular charge patterns on the PTFE surface by using KPFM, and the schematic of the relation between the diameter of the microdroplet before adsorption and the diameter of circular charge patterns. (*B*) The charge pattern generated on the PFTE surface by the evaporation of the microdroplets with different size (V is the average Kelvin potential). The charge patterns on the PTFE surface after approaching the (*C*) fog microdroplet (Movie S2), (*D*) positively charged fog microdroplet (Movie S3) and (*E*) negatively charge fog microdroplet (Movie S4) generated by the ultrasonic atomizer of 1.7 MHz frequency. The diameter distribution of (*F*) all the microdroplets, (*G*) positive microdroplets, and (*H*) negative microdroplets generated by the ultrasonic atomizer of 1.7 MHz frequency.

Further, an electric field was applied at the gap of the electrode to separate the positive and negative microdroplets, and the positive microdroplets and negative microdroplets are collected by two PTFE samples, respectively, as shown in Movies S3 and S4. The charge patterns of the positive microdroplets and negative microdroplets left on the PTFE surfaces are given in Fig. 2 *D* and *E*, respectively, and the diameter distributions of the positive microdroplets and negative microdroplets are shown in Fig. 2 *G* and *H*, respectively. It can be intuitively seen from Fig. 2 *D* and *E* that the negative microdroplets are significantly smaller than the positive microdroplets, and the average diameters of positive microdroplets and negative microdroplets are calculated to be 2.8 μm and 1.2 μm, respectively (Fig. 2 *G* and *H*), verifying the size-dependent charging of the microdroplets in ultrasonic atomization.

Calculation of Charges Carried by the Water Microdroplets. The average diameter of the microdroplet has been success measured to be 2.8 μm and 1.2 μm for positive microdroplets and negative microdroplets, respectively. If the relation between the terminal electrostatic velocity and the applied electric field is further determined, the amount of charge carried by the microdroplets can be calculated according to Eq. **4**. Here, the movement of the fog microdroplets (generated by the 1.7-MHz ultrasonic atomizer) in the different electric field various from 200 kV/m to 360 kV/m was investigated, as shown in Movies S1 and S5–S8 and Fig. 3 *A*–*C*. All the results confirm that there are both positive and negative microdroplets in the fog. And the moving velocity increased with the increase of the electric field strength as expected. By extracting the lateral terminal velocity of the fog microdroplets in the movies, the relations between the electric field strength and terminal electrostatic velocity of positive microdroplets and negative microdroplets were both established as shown in Fig. 3 *D* and *E*, respectively. It is shown that the terminal electrostatic velocity of both positive and negative microdroplets is proportional to the electric field strength, which is exactly consistent with Eq. **4**. By plugging the ratio of the terminal velocity to the electric field into Eq. **4**, the amount of positive charge carried by per microdroplet is calculated to be –2,384 e^- and the amount of negative charge carried by per microdroplet is 540 e^-.

Further, the charging of fog microdroplets generated by 2.4 MHz ultrasonic atomizer was investigated to verify the universality of our method and the size-dependent charge transfer in

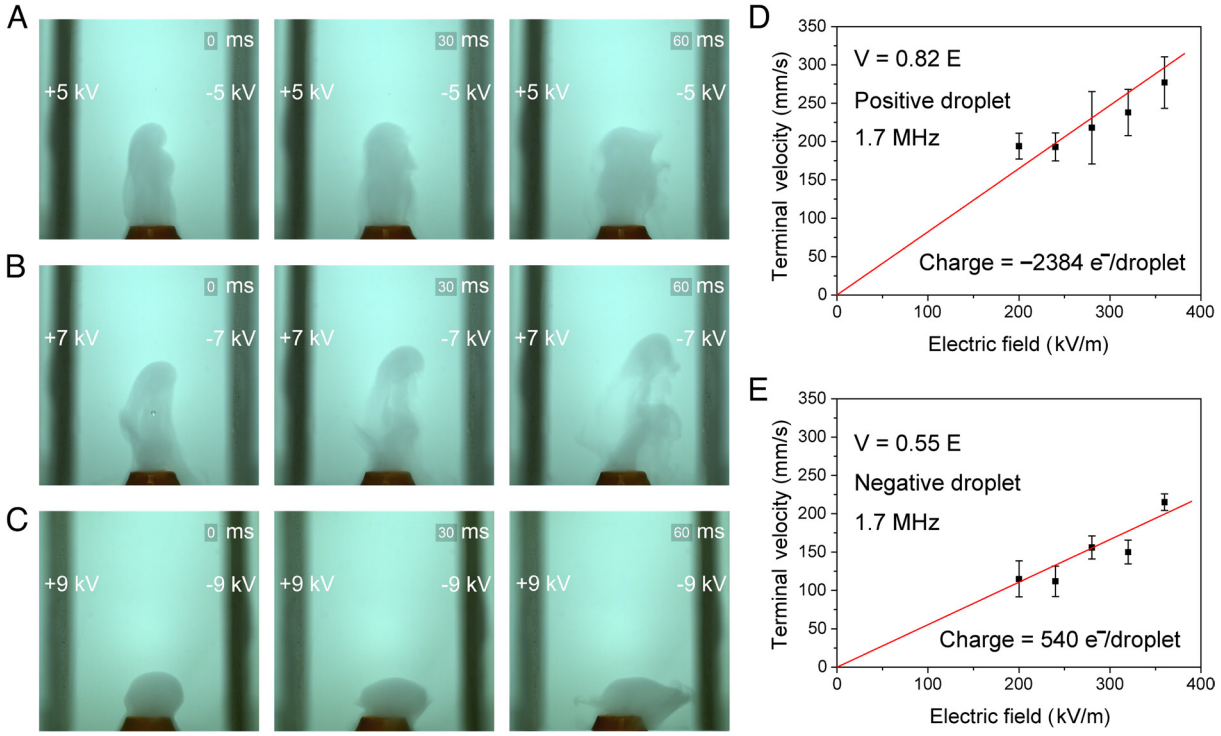

Fig. 3. Effect of electric field strength on the terminal electrostatic velocity. The movements of the fog microdroplets generated by a 1.7-MHz ultrasonic atomizer in the (*A*) 200 kV/m, (*B*) 280 kV/m, and (*C*) 360 kV/m electric fields. The relation between the terminal electrostatic velocity of (*D*) positive microdroplets, (*E*) negative microdroplets and the electric field.

ultrasonic atomization. As shown in Movies S9–S13 and Fig. 4*A*, there were also both positive microdroplets and negative microdroplets in the fog generated by the 2.4-MHz ultrasonic atomizer, and the moving velocity of the microdroplets increased with the increase of electric field. The microdroplets were collected by PTFE sample and the charge patterns on the PTFE surface are recorded by the KPFM method (*SI Appendix*, Fig. S4). The average diameter of the microdroplets generated by the 2.4-MHz ultrasonic atomizer can be seen as smaller than that generated by the 1.7-MHz ultrasonic atomizer. This is reasonable according to Eq. **6**, in which the average diameter of the microdroplets is proportional to $f^{-2/3}$. It is also shown in *SI Appendix*, Fig. S4 that positive microdroplets are usually larger than negative microdroplets in ultrasonic atomization with 2.4 MHz frequency. The diameter distribution of all the microdroplets, positive microdroplets, and negative microdroplets generated by the ultrasonic atomizer of 2.4 MHz frequency are shown in Fig. 4 *B*–*D*, and the average diameter of all the microdroplets was determined to be 2.2 μm in this case, which is also consistent with Eq. **6**. And the average diameters of positive and negative microdroplets were calculated to be 2.4 μm and 1.2 μm, respectively. With the same method used in the 1.7 MHz case, the relation between the terminal velocity of the microdroplet and the electric field in the 2.4 MHz case was established and the results are shown in Fig. 4 *E* and *F*. Plugging the ratio of the terminal velocity to the electric field and average diameter into Eq. **4**, the amount of positive charge carried by per microdroplet is calculated to be –1,864 e^- and the amount of negative charge carried by per microdroplet is 496 e^- in 2.4 MHz case. These results verified the universality of the size-dependent charging of microdroplets generated by ultrasonic atomization.

Size-Dependent Charge Transfer Model for the CE between Water Microdroplets. The experimental studies revealed an important fact that there are both positive microdroplets and negative microdroplets generated by ultrasonic atomization, and on average, the size of the positive microdroplets is usually larger than that of negative microdroplets. This implies that the negative charges transfer from the large microdroplet to the small microdroplet when the two microdroplets are separated by the ultrasonic stimulation, which is similar to the charge transfer between two chemically identical solid particles with different sizes. The mechanism of the size-dependent charge transfer between chemically identical solid particles has been widely discussed but it still remains ambiguous (4). A relative success explanation for the charge transfer between chemically identical solid particles is that the asymmetric size results in the asymmetric contact stress and asymmetric contact area involving in the multicollision CE, further leading to the transfer of negative charge from large particles to small particles (5). However, this explanation is not suitable for the liquid case. In ultrasonic atomization as shown in Fig. 5*A*, there are two modes of microdroplet formation. In one way, as shown in *SI Appendix*, Fig. S5, the water is directly thrown out of the water surface under the stimulation of ultrasonic wave to form microdroplets of different sizes. In another case, the thrown microdroplets are further separated into multiple microdroplets in different sizes under the action of ultrasonic wave (*SI Appendix*, Fig. S6). But in either case, it is impossible for microdroplets to make multiple contacts with each other owing to the fluidity of water and there is no asymmetric stress during their separation. Therefore, though the charging of chemically identical water microdroplets is similar to that of chemically identical solid particles, the charging mechanism of microdroplets needs to be discussed from a completely new perspective.

For simplification, we choose the second microdroplet formation mode to discuss the charging mechanism of microdroplets, as shown in *SI Appendix*, Fig. S6. The two microdroplets are chemically identical, the only difference between the two is size, which leads to different surface curvatures: the surface curvature of the

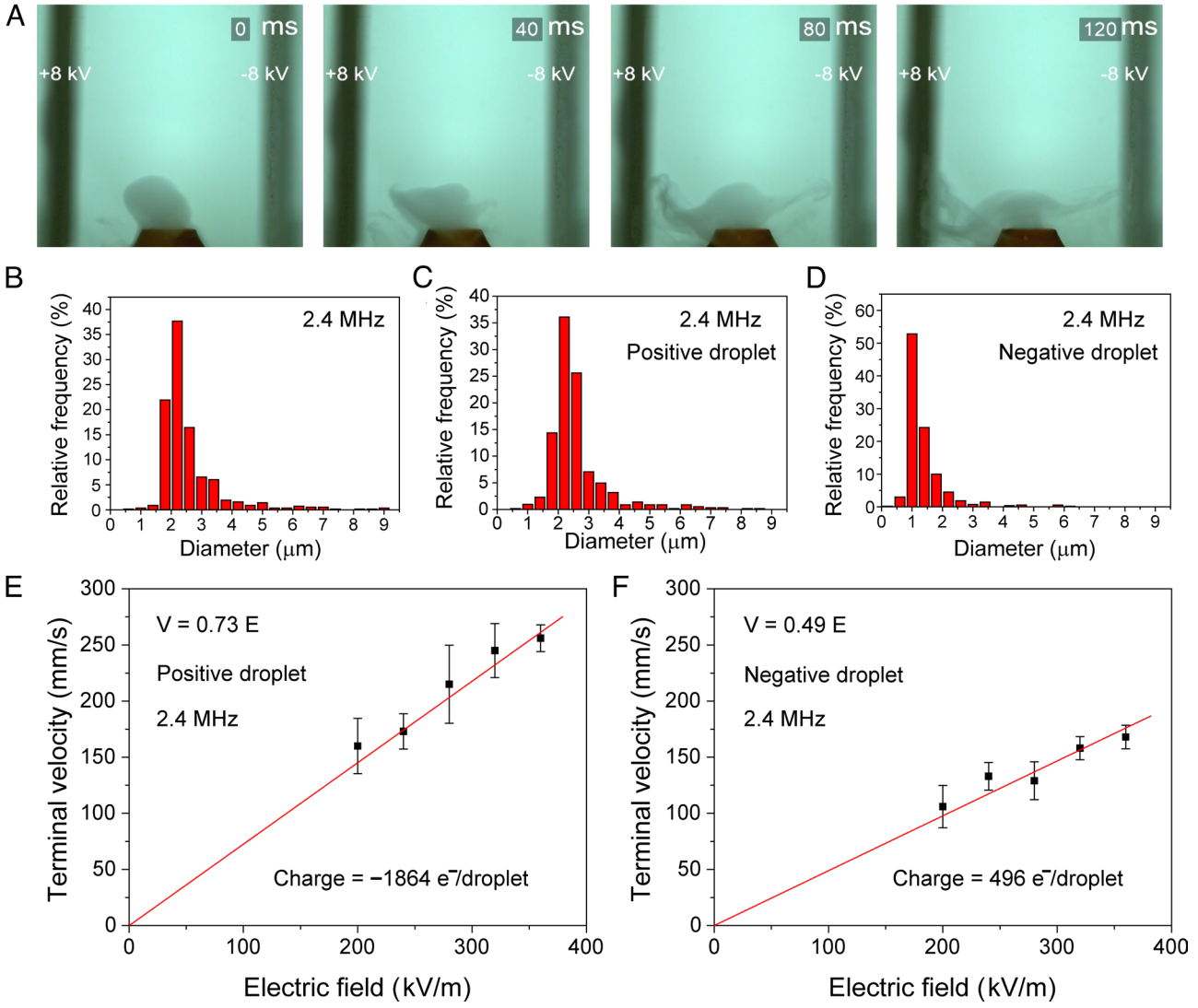

Fig. 4. The charging of fog microdroplets generated by a 2.4-MHz ultrasonic atomizer. (*A*) The movement of the fog microdroplets generated by the 2.4-MHz ultrasonic atomizer in 320 kV/m electric field. The diameter distribution of (*B*) all the microdroplets, (*C*) positive microdroplets, and (*D*) negative microdroplets generated by the ultrasonic atomizer of 2.4 MHz frequency. The relation between the terminal electrostatic velocity of (*E*) positive microdroplets, (*F*) negative microdroplets and the electric field.

large microdroplet is smaller than that of a small droplet. It was reported that the surface curvature of water will affect the net dipolar orientation of water molecules near the surface (51). Water molecules on the surface of large microdroplets with a small surface curvature tend to orient their hydrogen toward the vapor phase, while the water molecules on the small microdroplet surface tend to orient their hydrogen toward the water side. The orientation of the water molecules creates an electric field on the surface of the microdroplet, which affects the surface potential/energy of the microdroplet. Analogous to the work function of a metal, it can be inferred that it takes more work to move an electron to infinity from the inside of a relatively small microdroplet than a relatively large microdroplet. In other words, the surface potential (SP, corresponding to the work function of a metal) of the smaller microdroplet is larger than that of the larger microdroplet, as shown in Fig. 5*B*. Now, we have two trajectories to move a test charge, such as an electron, from the large microdroplet center to the center of the small microdroplet (*SI Appendix*, Fig. S6*A*). Trajectory 1 is going directly from inside the microdroplets; in trajectory 2, the electron leaves the surface of the large microdroplet and enters the surface of the small microdroplet. Because the SP of the small microdroplet is higher than that of the large microdroplet, the energy for the electron moving along trajectory 2 will be less than that moving along trajectory 1 (the energy difference is equal to the surface potential/energy difference between to the microdroplets). This cannot happen in real physics since it violates the law of conservation of energy. Thus, the difference in SP of the microdroplets will drive the negative charges transfer from the large microdroplet surface to the small microdroplet surface (*SI Appendix*, Fig. S6*B*), which establishes an electric field pointing from the large microdroplet surface to the small microdroplet surface, to compensate for the energy difference between the two trajectories (Fig. 5*C*), analogizing to the electron transfer between two metals with different work functions and formation of contact potential difference between two different metals. When the two microdroplets are completely separated by the ultrasonic wave, the positive charges stay on the large microdroplet and the negative charges stay on the surface of the small microdroplet, as observed in the experiments. We noted that the charge ratio between the positive and negative microdroplets is about 4:1, and the diameter ratio is about 2:1, which means that the amount of charge carried by the microdroplets is proportional to the surface area of spherical

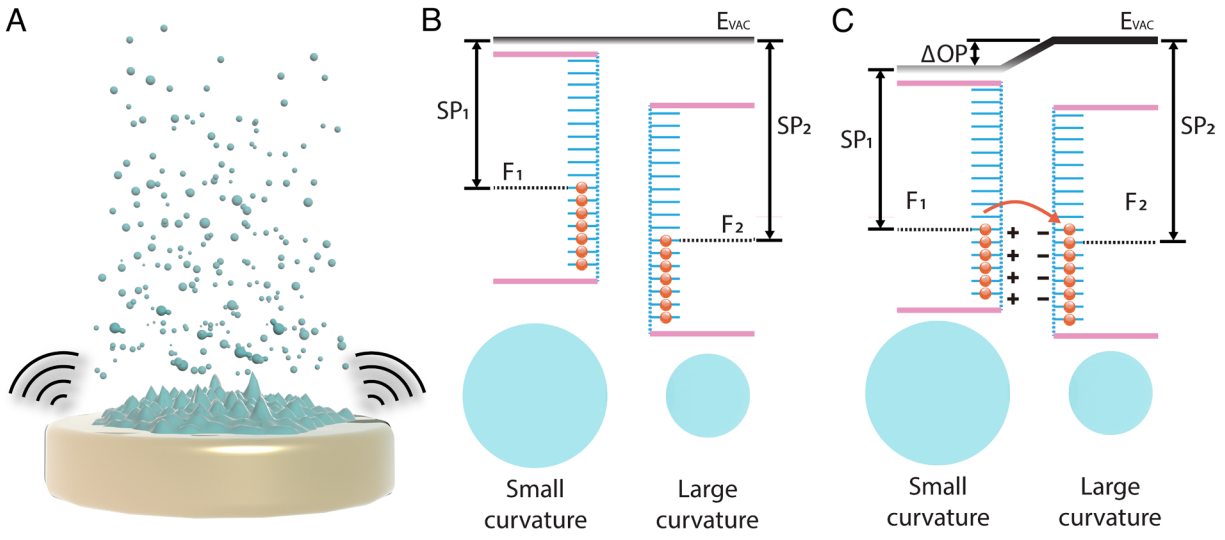

Fig. 5. The mechanism of asymmetric size–induced charge transfer between water microdroplets. (*A*) The schematic of the ultrasonic atomization. The band diagram of two separating water microdroplets with different surface curvatures (*B*) before charge transfer and (*C*) after charge transfer. SP is surface potential of the microdroplets, E_{VAC} is the vacuum energy level, ΔOP is the compensating potential generated by the transferred charges and F is the highest occupied energy level in the surface states of DI water.

microdroplets. This observation supports our charge transfer model, since the transferred charges are distributed on the surface of the microdroplets (*SI Appendix*, Fig. S6), so the amount of charge carried by the microdroplet is proportional to the surface area.

Although our interpretation is based on a hypothesis of dependence of surface energy on the surface curvature of the droplet, it needs to be pointed out that the collision between gas molecules and liquid surface during sonication may also result in charge transfer. It may be possible that the tuned surface potential by curvature may result in a reversion in charge transfer during collision. More experiments are needed to nail down the mechanism.

Discussion

Since the amount of charge carried by microdroplets has been measured, the electric field near the microdroplet surface can be further calculated and its effect on the chemical reaction can be evaluated. By using COMSOL simulation, the electric field strength near the surface of the isolated microdroplet with 2.6-μm diameter and carrying 2,000 e^- was calculated to be about ~10^6 V/m, as shown in *SI Appendix*, Fig. S7*A*. Such an electric field is unlikely to be strong enough to convert OH^- to OH* or promote a reaction that forms OH*. However, according to the mechanism described in Fig. 5, charge transfer occurs at the moment of separation of two microdroplets, so the electric field generated at the moment of separation needs to be considered. As shown in *SI Appendix*, Fig. S7*B*, the electric field strength between the two microdroplets at the moment of separation is calculated to be ~10^9 V/m, which is strong enough to convert OH^- to OH*. These results suggest that the spontaneous generation of H_2O_2 in the ultrasonic atomization case occurs during the separation of two micrometer-sized water droplets. In addition to the spontaneous generation of H_2O_2, our observation has general implications for microdroplet chemistry. The CE between identical water microdroplets may be one of the driving forces for the acceleration of reaction rates, since both the CE-induced electric field and the charge will shift the redox potential at the water–air interface (29–31, 52). Moreover, the size-dependent charge transfer between microdroplets gives a new perspective to understand the size-dependent chemical reaction rates in microdroplet chemistry (38, 53). According to the geometry, smaller droplets generally have a larger curvature difference between them, resulting in a larger charge transfer and larger redox potential shift, further inducing a greater change in chemical reaction rate.

Lastly, if the difference in microdroplet size can induce the oxidation of OH^- to OH*, it seems to mean that the smaller microdroplets in the nebulized systems are truly a remarkable oxidant, at least capable of oxidizing aromatics like benzene. However, the strong electric field is only present at the moment of microdroplet separation according to our simulation, which means that an isolated microdroplet does not have strong oxidation. In addition, it was reported that the unbalanced excess of OH^- will reduce the HO^*/OH^- redox potential at the liquid–gas interface (54), implying that the small microdroplet does not need to be a strong oxidant to oxidize OH^-. That is why we cannot observe the strong oxidation of microdroplets in the nebulized system.

In conclusion, a method for measuring the amount of charge carried by the fog water microdroplets was proposed based on the balance of electrostatic and drag forces. It was found that there are both positive and negative microdroplets generated by ultrasonic atomization. By measuring the diameter distribution of the microdroplets, it turned out that the diameter of the positive microdroplets is usually larger than that of the negative microdroplets, which implied that the negative charges transfer from large microdroplets to small microdroplets in the ultrasonic atomization. A model analogous to the contact electron transfer between different metals was proposed for the charging of microdroplets, in which the curvature-induced surface potential differences are suggested to be responsible for the charge transfer between microdroplets. The results show that the electric field strength between two microdroplets with opposite charges during separation reached ~10^9 V/m, which is strong enough to convert OH^- to OH*, further generating H_2O_2. The findings provide experimental evidence for the CE-induced spontaneous generation of H_2O_2 in microdroplets and also have implications in the sonochemistry, microdroplet chemistry and chemical engineering, etc., in which the liquid microdroplets are involved in the chemical reactions.

Materials and Methods

Materials. The PTFE layers of 100 nm were deposited on high-doped SI by magnetron sputtering under room temperature, and the DI water with a resistivity of 18.2 MΩ·cm was produced by a deionizer (HHitech, China).

Calculation of Terminal Velocity. The terminal velocity of microdroplets was obtained by dividing the traveling distance by time. Some calculation details need to be clarified. The traveling distance and traveling time of the microdroplets were extracted from the movies at the beginning of the application of the electric field to avoid the effects of turbulence. *SI Appendix*, Fig. S8 gives two examples of terminal velocity calculation (terminal velocity of microdroplets generated by 2.4 MHz, under 200 kV/m and 300 kV/m). It is shown that within a few hundred milliseconds after the application of the electric field, the microdroplets did not reach the metal plate, and no obvious turbulence is generated. The traveling distance and traveling time of the microdroplets can be obtained, and then the terminal velocity can be calculated.

AFM Experiments. The surface potential experiments were performed on a commercial AFM equipment Dimension Icon (Bruker, USA) in a glove box filled with nitrogen. SCM-PIT (Bruker, USA; tip radius 25 nm) was used as the Pt-coated tip in the charging experiments and surface potential measurement. The surface potential of the PTFE sample was measured by using KPFM mode, in which the topography of the sample was measured by tapping mode in the first pass, and the surface potential was measured in the second pass. In the KPFM mode, the lift height in the second pass was 50 nm and the amplitude setpoint was set to 350 mV.

COMSOL Simulation. The numerical simulation was conducted with COMSOL software with electrostatics physics. 3D models were built and two cases were run: 1) merely a 2.6-μm droplet and 2) one 2.6-μm and four 1.2-μm droplets. The dimensions of the simulation zone are 30 × 70 × 100 μm with an infinite element domain as the outer boundary layer condition. Water was used as the droplet material and floating potential was used as the boundary condition of the droplet. Then, −600 (negative) and 2,400 (positive) were used as the charge number of 1.2- and 2.6-μm droplets, respectively. Physics-controlled mesh was used with extremely fine element size. In case 2, the 2.6-μm droplet was surrounded uniformly by four droplets in the diameter of 1.2 μm, whose centers were all located in the xy plane. Distance between the small and large droplets was 1 nm.

Data, Materials, and Software Availability. All study data are included in the article and/or supporting information.

ACKNOWLEDGMENTS. Research was supported by the National Natural Science Foundation of China (Grant No. 52005044), National Key R & D Project from Minister of Science and Technology (2021YFA1201601).

Author affiliations: [a]Beijing Institute of Nanoenergy and Nanosystems, Chinese Academy of Sciences, Beijing 100083, People's Republic of China; [b]School of Nanoscience and Technology, University of Chinese Academy of Sciences, Beijing 100049, People's Republic of China; [c]School of Materials Science and Engineering, Georgia Institute of Technology, Atlanta, GA 30332–0245; and [d]Yonsei Frontier Lab, Yonsei University, Seoul 03722, Republic of Korea

1. Y. Zhang *et al.*, Electric field and humidity trigger contact electrification. *Phys. Rev. X* **5**, 011002 (2015).
2. W. Wei, Z. Gu, Electrification of particulate entrained fluid flows-mechanisms, applications, and numerical methodology. *Phys. Rep.* **600**, 1–53 (2015).
3. P. Krehbiel *et al.*, Upward electrical discharges from thunderstorms. *Nat. Geosci.* **1**, 233–237 (2008).
4. D. Lacks, R. Sankaran, Contact electrification of insulating materials. *J. Phys. D: Appl. Phys.* **44**, 453001 (2011).
5. J. Kok, D. Lacks, Electrification of granular systems of identical insulators. *Phys. Rev. E* **79**, 051304 (2009).
6. S. Waitukaitis, V. Lee, J. Pierson, S. Forman, H. Jaeger, Size-dependent same material tribocharging in insulating grains. *Phys. Rev. Lett.* **122**, 218001 (2014).
7. K. Huang, Z. Wei, R. Cooks, Accelerated reactions of amines with carbon dioxide driven by superacid at the microdroplet interface. *Chem. Sci.* **12**, 2242 (2021).
8. L. Qiu, R. Cooks, Simultaneous and spontaneous oxidation and reduction in microdroplets by the water radical cation/anion pair. *Angew. Chem. Int. Ed. Engl.* **61**, e202210765 (2022).
9. P. Basuri, L. Gonzalez, N. Morato, T. Pradeep, R. Cooks, Accelerated microdroplet synthesis of benzimidazoles by nucleophilic addition to protonated carboxylic acids. *Chem. Sci.* **11**, 12686 (2020).
10. A. Huebner *et al.*, Microdroplets: A sea of application? *Lab Chip* **8**, 1244–1254 (2008).
11. T. Taniguchi, T. Torii, T. Higuchi, Chemical reactions in microdroplets by electrostatic manipulation of droplets in liquid media. *Lab Chip* **2**, 19–23 (2002).
12. E. Zdrali, Y. Chen, H. Okur, D. Wilkins, S. Roke, The molecular mechanism of nanodroplet stability. *ACS Nano* **11**, 12111–12120 (2017).
13. E. Zdrali, H. Okur, S. Roke, Specific ion effects at the interface of nanometer-sized droplets in water: Structure and stability. *J. Phys. Chem. C* **123**, 16621–16630 (2019).
14. X. Yan, R. Bain, R. Cooks, Organic reactions in microdroplets: Reaction acceleration revealed by mass spectrometry. *Angew. Chem. Int. Ed. Engl.* **55**, 12960–12972 (2016).
15. L. Zhao *et al.*, Sprayed water microdroplets containing dissolved pyridine spontaneously generate pyridyl anions. *Proc. Natl. Acad. Sci. U.S.A.* **119**, e2200991119 (2022).
16. P. Basuri, J. Kumar, S. Das, T. Pradeep, Accelerated non-enzymatic fatty acid esterification during microdroplet collision: A method for enhanced sustainability. *ACS Sustainable Chem. Eng.* **10**, 8577–8587 (2022).
17. M. Lopez, M. Martins-Costa, Disentangling reaction rate acceleration in microdroplets. *Phys. Chem. Chem. Phys.* **24**, 29700 (2022).
18. J. Ghosh, J. Mendoza, R. Cooks, Accelerated and concerted Aza-Michael addition and SuFEx reaction in microdroplets in unitary and high-throughput formats. *Angew. Chem. Int. Ed. Engl.* **61**, e202214090 (2022).
19. A. Fallah-Araghi *et al.*, Enhanced chemical synthesis at soft interfaces: A universal reaction-adsorption mechanism in microcompartments. *Phys. Rev. Lett.* **112**, 028301 (2014).
20. Y. Yang *et al.*, A high-throughput screening method for determining the optimized synthesis conditions of quinoxaline derivatives using microdroplet reaction. *Front. Chem.* **8**, 789 (2020).
21. D. Holden, N. Morato, R. Cooks, Aqueous microdroplets enable abiotic synthesis and chain extension of unique peptide isomers from free amino acids. *Proc. Natl. Acad. Sci. U.S.A.* **119**, e2212642119 (2022).
22. H. Nie *et al.*, High-yield gram-scale organic synthesis using accelerated microdroplet/thin film reactions with solvent recycling. *Chem. Sci.* **11**, 2356 (2020).
23. A. Li, Q. Luo, S. Park, R. Cooks, Synthesis and catalytic reactions of nanoparticles formed by electrospray ionization of coinage metals. *Angew. Chem. Int. Ed. Engl.* **53**, 3147–3150 (2014).
24. D. Sarkar *et al.*, Metallic nanobrushes made using ambient droplet sprays. *Adv. Mater.* **28**, 2223–2228 (2016).
25. F. Kovacik, H. Okur, N. Smolentsev, R. Scheu, S. Roke, Hydration mediated interfacial transitions on mixed hydrophobic/hydrophilic nanodroplet interfaces. *J. Chem. Phys.* **149**, 234704 (2018).
26. E. Zdrali, M. Baer, H. Okur, C. Mundy, S. Roke, The diverse nature of ion speciation at the nanoscale hydrophobic/water interface. *J. Phys. Chem. B* **123**, 2414–2423 (2019).
27. R. Scheu, Y. Chen, M. Subinya, S. Roke, Stern layer formation induced by hydrophobic interactions: A molecular level study. *J. Am. Chem. Soc.* **135**, 19330–19335 (2013).
28. Z. Wei, Y. Li, R. Cooks, X. Yan, Accelerated reaction kinetics in microdroplets: Overview and recent developments. *Annu. Rev. Phys. Chem.* **71**, 31–51 (2020).
29. J. Heindel, H. Hao, R. LaCour, T. Head-Gordon, Spontaneous formation of hydrogen peroxide in water microdroplets. *J. Phys. Chem. Lett.* **13**, 10035–10041 (2022).
30. H. Hao, I. Leven, T. Head-Gordon, Can electric fields drive chemistry for an aqueous microdroplet? *Nat. Commun.* **13**, 280 (2022).
31. H. Xiong, J. Lee, R. Zare, W. Min, Strong electric field observed at the interface of aqueous microdroplets. *J. Phys. Chem. Lett.* **11**, 7423–7428 (2020).
32. C. Chamberlayne, R. Zare, Microdroplets can act as electrochemical cells. *J. Chem. Phys.* **156**, 054705 (2022).
33. S. Lin, X. Chen, Z. L. Wang, Contact electrification at the liquid-solid interface. *Chem. Rev.* **122**, 5209–5232 (2022).
34. T. Kakeshpour, B. Metaferia, R. Zare, A. Bax, Quantitative detection of hydrogen peroxide in rain, air, exhaled breath, and biological fluids by NMR spectroscopy. *Proc. Natl. Acad. Sci. U.S.A.* **119**, e2121542119 (2022).
35. M. Mehrgardi, M. Mofidfar, R. Zare, Sprayed water microdroplets are able to generate hydrogen peroxide spontaneously. *J. Am. Chem. Soc.* **144**, 7606–7609 (2022).
36. B. Chen *et al.*, Water-solid contact electrification causes hydrogen peroxide production from hydroxyl radical recombination in sprayed microdroplets. *Proc. Natl. Acad. Sci. U.S.A.* **119**, e2209056119 (2022).
37. N. Musskopf, A. Gallo, P. Zhang, J. Petry, H. Mishra, The air-water interface of water microdroplets formed by ultrasonication or condensation does not produce H_2O_2. *J. Phys. Chem. Lett.* **12**, 11422–11429 (2021).
38. J. Lee *et al.*, Spontaneous generation of hydrogen peroxide from aqueous microdroplets. *Proc. Natl. Acad. Sci. U.S.A.* **116**, 19294–19298 (2019).
39. J. Lee *et al.*, Condensing water vapor to droplets generates hydrogen peroxide. *Proc. Natl. Acad. Sci. U.S.A.* **117**, 30934–30941 (2020).
40. P. Mehrani, H. Bi, J. Grace, Electrostatic charge generation in gas-solid fluidized beds. *J. Electrostat.* **63**, 165–173 (2005).
41. S. Soh, S. Kwok, H. Liu, G. Whitesides, Contact de-electrification of electrostatically charged polymers. *J. Am. Chem. Soc.* **134**, 20151–20159 (2012).
42. Z. Tang, S. Lin, Z. L. Wang, Quantifying contact electrification induced charge transfer on a liquid droplet after contacting with a liquid or solid. *Adv. Mater.* **33**, 2102886 (2021).
43. R. Millikan, The isolation of an ion, a precision measurement of its charge, and the correction of Stokes's law. *Science* **32**, 436–448 (1910).
44. R. Jones, The Millikan oil-drop experiment-making it worthwhile. *Am. J. Phys.* **63**, 970 (1995).
45. J. Nauruzbayeva *et al.*, Electrification at water-hydrophobe interfaces. *Nat. Commun.* **11**, 5285 (2020).
46. B. Liu, D. Pui, On the performance of the electrical aerosol analyzer. *J. Aerosol Sci.* **6**, 249–264 (1975).
47. W. Hinds, Y. Zhu, *Aerosol Technology: Properties, Behavior, and Measurement of Airborne Particles* (John Wiley & Sons, 2022).

48. J. Kim, G. Mulholland, S. Kukuck, D. Pui, Slip correction measurements of certified PSL nanoparticles using a nanometer differential mobility analyzer (nano-DMA) for Knudsen number from 0.5 to 83. *J. Res. Natl. Inst. Stan.* **110**, 31–54 (2005).
49. S. Lin, L. Xu, A. Wang, Z. L. Wang, Quantifying electron-transfer in liquid-solid contact electrification and the formation of electric double-layer. *Nat. Commun.* **11**, 399 (2020).
50. H. Naidu, O. Kahraman, H. Feng, Novel applications of ultrasonic atomization in the manufacturing of fine chemicals, Pharmaceuticals, and medical devices. *Ultrason. Sonochem.* **86**, 105984 (2022).
51. R. Cooper, J. O'Brien, T. Chang, E. Williams, Structural and electrostatic effects at the surfaces of size and charge selected aqueous nanodrops. *Chem. Sci.* **8**, 5201 (2017).
52. J. Lee, S. Banerjee, H. Nam, R. Zare, Acceleration of reaction in charged microdroplets. *Q. Rev. Biophys.* **48**, 437–444 (2015).
53. E. Adams *et al.*, Proton traffic jam: Effect of nanoconfinement and acid concentration on proton hopping mechanism. *Angew. Chem. Int. Ed. Engl.* **60**, 25419–25427 (2021).
54. Y. Vogel *et al.*, The corona of a surface bubble promotes electrochemical reactions. *Nat. Commun.* **11**, 6323 (2020).